

1 **Isotopic apportionment of sulfate aerosols between natural**  
2 **and anthropogenic sources in the outflow of South Asia**

3  
4 Sean Clarke<sup>1</sup>, Henry Holmstrand<sup>1</sup>, Krishnakant Budhavant<sup>2,3</sup>, Manoj Remani<sup>1</sup>, Sophie  
5 Haslett<sup>1</sup>, Katerina Rodiouchkina<sup>4,5</sup>, Ellen Kooijman<sup>6</sup>, Örjan Gustafsson<sup>1</sup>

6 <sup>1</sup> Department of Environmental Science, Stockholm University, 11418 Stockholm, Sweden.

7 <sup>2</sup> Maldives Climate Observatory at Hanimaadhoo, H. Dh. Hanimaadhoo, The Maldives

8 <sup>3</sup> Divecha Centre for Climate Change, Indian Institute of Science, Bangalore, Karnataka 560012, India

9 <sup>4</sup> Division of Geosciences, Luleå University of Technology, 971 87 Luleå, Sweden

10 <sup>5</sup> ALS Scandinavia AB, 977 75, Luleå, Sweden

11 <sup>6</sup> Department of Geosciences, Swedish Museum of Natural History, Box 50 007, Stockholm, SE-104 05, Sweden

12  
13 *Corresponding authors: [Orjan.Gustafsson@aces.su.se](mailto:Orjan.Gustafsson@aces.su.se); [Sean.Clarke@aces.su.se](mailto:Sean.Clarke@aces.su.se)*

14

15 **Abstract**

16 Sulfate aerosols cool the climate and thus temporarily mask climate warming, but at a cost to air quality. Their  
17 short atmospheric lifetime leads to heterogeneous global coverage, with sulfate concentrations over South Asia  
18 being especially elevated and continuing to increase. It remains challenging to constrain the relative importance  
19 of different emission sources due to poor observational coverage and uncertainties in bottom-up technology-based  
20 emission estimates. The stable sulfur isotope composition ( $\delta^{34}\text{S-SO}_4^{2-}$ ) quantitatively distinguishes natural and  
21 anthropogenic sources. This study aimed to constrain the sources of sulfate arriving at the Maldives Climate  
22 Observatory Hanimaadhoo (MCOH), which is ideally situated for intercepting the outflow from airsheds over the  
23 Indian subcontinent. The results show that anthropogenic sources of sulfate contributed  $934 \pm 141$  %,  $878 \pm 109$   
24 %, and  $667 \pm 123$  % in winter (post-monsoon), spring (pre-monsoon), and summer (monsoon), respectively. There  
25 was also a moderate to strong correlation ( $r^2 = 0.759$ ,  $p \ll 0.05$ ,  $n = 7$ ) between continental anthropogenic (winter  
26 and spring) sulfate ( $\delta^{34}\text{S}$ ) and black carbon aerosols from fossil fuel combustion (pinpointed by  $\Delta^{14}\text{C}$ ). This study  
27 provides improved constraints on sulfate sources for South Asia – a key region for aerosol pollution and aerosol  
28 masking of climate warming.

29

30

31

32

## 33 **1 Introduction**

34 Anthropogenic aerosols cause substantial net negative climate forcing, which is currently attenuating the warming  
35 caused by the emissions of greenhouse gases. Sulfate aerosols represent the largest component of this aerosol-  
36 induced masking of climate warming and the health-affecting deterioration of air quality. Sulfate aerosols are  
37 primarily secondary aerosols formed from the oxidation (via H<sub>2</sub>O<sub>2</sub>, O<sub>3</sub>, OH, transition metals, NO<sub>2</sub>) of sulfur  
38 dioxide, hydrogen sulfide, and sulfur-bearing organic substances, emitted from numerous natural and  
39 anthropogenic sources (e.g., Berresheim et al., 2002; Szopa et al., 2021). These aerosols then alter the climate  
40 through the direct (scattering of light) and indirect effects (primarily alteration of cloud properties), leading to a  
41 net cooling effect (e.g., Charlson et al., 1991; Szopa et al., 2021).

42 These climatic effects are associated with the ubiquitous presence of sulfate aerosols in the atmosphere, leading  
43 to an effective radiative forcing (ERF) of -0.94 Wm<sup>-2</sup> [-1.63 to -0.25 Wm<sup>-2</sup>] (Szopa et al., 2021). However, the  
44 aerosols' short atmospheric lifetime (1-2 weeks) is expected to lead to a rapid readjustment once emissions change.

45 There have been regional reductions in sulfate emissions in North America and Europe for several decades. While  
46 these reductions are significant environmental legislative successes, emission patterns shifted eastwards towards  
47 Asia. The rise in emissions in East Asia led to a brief increase in global emissions at the start of the 21<sup>st</sup> century  
48 (McDuffie et al., 2020). However, subsequent successful mitigation efforts primarily in China have dramatically  
49 decreased sulfate loadings in the recent decade (McDuffie et al., 2020). The emissions from India surpassed those  
50 of China at the end of the last decade (Li et al., 2017); South Asia is currently the epicenter of sulfate emissions,  
51 with emissions still believed to be on the rise (McDuffie et al., 2020).

52 South Asia experienced rapid industrialization and economic growth in the latter part of the 20<sup>th</sup> century that have  
53 continued into the present day, with the unintended consequence of high aerosol emissions. These loadings are  
54 shown by the increasing trend over the last few decades in the aerosol optical depth (AOD), with sulfate being a  
55 large contributor to this increase (Aas et al., 2019; Gupta et al., 2023). These high aerosol loadings must be  
56 addressed as they are a major health and environmental burden on South Asia, which is home to almost a quarter  
57 of the world's population (Lelieveld et al., 2020). However, our knowledge about sulfate sources and emissions  
58 remains uncertain with notable disparities between estimates from emission inventories and from remote sensing  
59 (Elguindi et al., 2020; Sharma and Kumar, 2016). The understanding of sulfate emissions is further hampered by  
60 uncertainties in natural emissions, such as oceanic dimethyl sulfide (DMS), which has seasonal and regional  
61 emission fluctuations ranging by a factor of 10-100 (Norman et al., 1999, 2004; Shenoy and Kumar, 2007). These  
62 uncertainties lead to large variations in estimates of natural versus anthropogenic contributions, especially in  
63 locations surrounded by oceans such as South Asia (Norman et al., 1999, 2004; Shenoy and Kumar, 2007).  
64 Quantitative top-down source-diagnostic isotopic composition, in combination with consideration of air-mass  
65 origins, presents an opportunity to quantitatively apportion the relative contributions from anthropogenic and  
66 natural sources of sulfate for the wider receptor atmosphere of South Asia.

67

68 Isotopic composition allows for the quantitative separation of natural versus anthropogenic sources of sulfate  
69 through distinct source end-member compositions (source fingerprints). The use of δ<sup>34</sup>S for separating natural vs

70 anthropogenic sources is established, with a few pioneering studies now also in South Asia (Dasari and Widory,  
71 2024; Rastogi et al., 2020; Sawlani et al., 2019).

72 This study employs isotopic  $\delta^{34}\text{S}$  source apportionment of  $\text{SO}_4^{2-}$  to quantify the anthropogenic sulfate  
73 contributions to the expansive airshed outflow from South Asia (representative of the wider system of the regional  
74 aerosol-climate effect). The present study has a much wider footprint and longer time coverage than earlier studies  
75 in the region. Distinguishing the relative source contributions of the climate-affecting sulfate in the South Asia  
76 region provides guidance for future mitigation strategies and also provides observation-based constraints useful  
77 for climate models.

78

## 79 **2. Methods**

### 80 **2.1 Site description and meteorological context**

81 South Asia encompasses several climate zones with its climate being primarily driven by the South Asian  
82 monsoon. The monsoon season marks the onset of frequent precipitation events and the reversal of the prevailing  
83 northerly winds. The southerly monsoon winds transport air masses from the Indian Ocean to the continent.  
84 Seasonal oscillation also occurs in the zonal (east-west) wind component, with stronger easterlies during winter  
85 and autumn (from the Bay of Bengal), and more westerly flow in spring (from the Arabian Sea).

86 Meteorologically, this leads to air masses from the high-emission region of the Indo-Gangetic Plain (IGP) being  
87 transported into the Bay of Bengal in winter/autumn with dispersal of their anthropogenic load also over the  
88 northern Indian Ocean (see Fig. 1). The IGP is a fertile, densely populated and highly industrialized region  
89 spanning several countries. The IGP contributes the highest aerosol loading in South Asia and strongly impacts  
90 aerosol loadings far out over the Indian Ocean (Aswini et al., 2020; Budhavant et al., 2024; Nair et al., 2023;  
91 Ramanathan et al., 2001; Verma et al., 2012).

92 The Maldives Climate Observatory at Hanimaadhoo (MCOH;  $6^\circ 46' 34''\text{N}$ ,  $73^\circ 10' 59''\text{E}$ ; tower inlet at 15 m agl) is  
93 ideally situated for intercepting air masses arriving from the polluted and polluting IGP, the subcontinent at large,  
94 and additionally from the open Indian Ocean during the summer (see Fig. 1). As the IGP is the key source region  
95 of anthropogenic aerosols, two additional sites were chosen in this emission region to constrain its anthropogenic  
96 sulfate signature. These sites were the Delhi branch of the Indian Institute of Tropical Meteorology (IITM-Delhi;  
97  $28^\circ 35'\text{N}$ ,  $77^\circ 12'\text{E}$ ; 15 m agl) and the Bangladesh Climate Observatory Bhola (BCOB;  $22^\circ 17' 00''\text{N}$ ,  $90^\circ 42' 36''\text{E}$ ,  
98 10 m agl) (see Fig. 1). Detailed information on the observatory sites can be found in previous studies (e.g., Bikkina  
99 et al., 2019; Dasari et al., 2019).

### 100 **2.2 Collection of aerosols**

101 Samples for stable sulfur isotope measurements of sulfate in this study were hence collected from three sites in  
102 South Asia. The urban  $\text{PM}_{2.5}$  filters (47 mm diameter quartz filters, Millipore) were collected from the IITM-Delhi  
103 in the winter of 2016 (January and February) using a high-volume sampler (APM 550 Envirotech, flow rate = 1  
104  $\text{m}^3 \text{hr}^{-1}$ , time = 12 hours). The IGP outflow  $\text{PM}_{2.5}$  filters were collected at BCOB in the winter of 2016 (January),  
105 using a high-volume sampler (model DH77, DIGITEL A.G., Switzerland, flow rate =  $500 \text{L min}^{-1}$ , time = 24  
106 hours). The integrating filters of the South Asian outflow, intercepted over the Indian Ocean, were collected at  
107 MCOH with sample dates spanning several years (winter = 2016, summer = 2013-2015, spring = 2013) (winter =

108 PM<sub>1</sub>, spring and summer = PM<sub>2.5</sub>) using a high-volume sampler (model DH77, DIGITEL A.G., Switzerland, flow  
109 rate = 500 L min<sup>-1</sup>, time = 24 hours). Detailed information on the collection of aerosol samples can be found in  
110 previous studies (e.g., Kirillova et al., 2013, 2014).

### 111 2.3 Ionic concentrations

112 Ionic concentrations (Cl<sup>-</sup>, Br<sup>-</sup>, NO<sub>2</sub><sup>-</sup>, NO<sub>3</sub><sup>-</sup>, PO<sub>4</sub><sup>3-</sup>, SO<sub>4</sub><sup>2-</sup>, Na<sup>+</sup>, NH<sub>4</sub><sup>+</sup>, K<sup>+</sup>, Mg<sup>2+</sup>, Ca<sup>2+</sup>) were measured using a  
113 Dionex Aquion ion chromatography (IC) system (Thermo Finnigan LLC, [Dionex IonPac CS12A](#)) anion ([Dionex](#)  
114 [IonPac AS22 fast](#)). Cut-outs (1-4 cm<sup>2</sup>) of the filter samples were dissolved in 10 mL of Milli-Q water and analyzed  
115 with a flow rate of 1 mL min<sup>-1</sup>. Standards and field blanks were used to ensure quality control and minimize  
116 external influences.

117 The sea spray fraction of SO<sub>4</sub><sup>2-</sup> was removed following (Keene et al., 1986), as shown in Eq. (1):

$$118 \text{ nssSO}_4^{2-} = [\text{SO}_4^{2-}] - \left( \frac{[\text{SO}_4^{2-}]}{[\text{Na}^+]} \right)_{\text{sea}} \times [\text{Na}^+] \quad (1)$$

119 The nss-SO<sub>4</sub><sup>2-</sup> is the non-sea salt sulfate, with the [mass](#) ratio of sulfate to sodium from sea water being 0.253  
120 taken from (Keene et al., 1986). Seawater is enriched in sulfate due to long-term accumulation. This results in  
121 natural emissions of sulfate aerosols from sea spray, which must be accounted for to enable accurate source  
122 apportionment of nss-SO<sub>4</sub><sup>2-</sup>.

123

### 124 2.4 Isotopic analysis

#### 125 2.4.1 Analysis of δ<sup>34</sup>S

126 The determination of the δ<sup>34</sup>S composition of aerosols on 17 carefully selected samples was performed following  
127 the method described in detail in Rodiouchkina, 2018. Filter cut-outs were placed in polypropylene tubes and  
128 Milli-Q water was added to extract the sulfate (5 h in an ultrasonic bath). Sulfur was then isolated using anion  
129 exchange chromatography (AG 1-X8, analytical grade, 200-400 mesh, chloride form, Bio-Rad Laboratories,  
130 USA). The standards (S1, S3, and S4 from IAEA, Austria) and samples were then diluted to an S concentration  
131 of 2 µg mL<sup>-1</sup> before being run in a solution matrix of 0.3 M HNO<sub>3</sub> (sub-boiled). Silicon (Si) was added to all  
132 solutions [as ammonium hexafluorosilicat \(NH<sub>4</sub>\)<sub>2</sub>SiF<sub>6</sub>](#), at a concentration ratio of 1:1 (S:Si, µg mL<sup>-1</sup>:µg mL<sup>-1</sup>) for  
133 internal standardization. Additionally, sodium (Na) was added [as sodium carbonate \(Na<sub>2</sub>CO<sub>3</sub>\)](#) at a molar ratio of  
134 2 (Na/S) to all measurement solutions. The measurements were carried out using a multi-collector inductively  
135 coupled plasma mass spectrometer (MC-ICP-MS, Nu Plasma II, Nu Instruments, UK) and run-in dry plasma mode  
136 using a desolvator (Aridus II, CETAC, USA) at the Vegacenter facility of the Swedish Museum of Natural  
137 History, Stockholm, Sweden. Detailed descriptions and typical operating parameters can be found in  
138 Rodiouchkina, 2018. For instrument settings and parameters see Method S1.

139

#### 140 2.4.2 Analysis of radiocarbon (Δ<sup>14</sup>C) composition in Black Carbon (BC)

141 A total of 14 samples for Δ<sup>14</sup>C were prepared for dual isotopic analysis of combustion-derived BC (MCOH spring  
142 = 2, MCOH summer = 3, BCOB = 3, MCOH winter = 6). The winter samples comprise data taken from Dasari et  
143 al., 2020. Inorganic carbonates were removed by acid fumigation (12 M HCl) for 24 h, then the samples were  
144 dried at 60 °C for 1 h. The samples were subjected to thermal-oxidation separation of OC from BC using a TOT

145 analyzer (Thermal Optical Transmittance, Sunset Laboratory, Tigard, Oregon, USA) and the resulting carbon  
 146 dioxide derived from the BC fraction was trapped using a custom-built system described and extensively tested  
 147 earlier (e.g., Andersson et al., 2015; Chen et al., 2013; Winiger et al., 2015). The trapped CO<sub>2</sub> from the BC fraction  
 148 was then sent to the collaborating Accelerator Mass Spectrometry facility (AMS) at Uppsala University (Sweden)  
 149 for  $\Delta^{14}\text{C}$  isotopic analysis. The source apportionment was calculated using Eq. (2) and Eq. (3), with end-member  
 150 values taken from the literature (Andersson et al., 2015; Bikkina et al., 2019).

$$151 \quad \Delta^{14}\text{C}_{BC} = \left[ F_m \times e^{\frac{-(x_{\text{year}}-1954)}{8267}} - 1 \right] \times 1000 \quad (2)$$

152

$$153 \quad \Delta^{14}\text{C}_{BC} = \Delta^{14}\text{C}_{biomass} \times F_{bio-BC} + \Delta^{14}\text{C}_{fossil} \times (1 - F_{bio-BC}) \quad (3)$$

154

## 155 **2.5 Model for apportioning between natural and anthropogenic sulfur input**

156 The approach to apportion natural versus anthropogenic sulfate was carried out in several steps. First, the data  
 157 were corrected for the minor contribution from sea spray based on the well-known isotopic composition of sea  
 158 water using Eq. (4). The sample MCOH PM<sub>1</sub>\_13-14/01/2016 was corrected using the fraction of non-sea salt  
 159 contribution to tot-SO<sub>4</sub> from the other samples (98.9 ± 0.2 %) due to sample depletion.

$$160 \quad \delta^{34}\text{S}_{nss} = \left( \delta^{34}\text{S} - \left( \frac{100 - F_{\%nssSO_4}}{100} \right) \times \delta^{34}\text{S}_{sea\ water} \right) \div \frac{\%nssSO_4}{100} \quad (4)$$

161 The isotopic composition of  $\delta^{34}\text{S}_{sea\ water}$  is +21 ± 0.2 ‰ from Böttcher et al., 2007 and Rees et al., 1978. The  
 162 percentage of nss-SO<sub>4</sub><sup>2-</sup> is determined from Eq. (1).

163 After this correction, the nss- $\delta^{34}\text{S}$  was used in a binary model to apportion the relative contributions from  
 164 anthropogenic-fossil sources (e.g., ship emissions/IGP sources) vs the marine biogenic (DMS) source, using Eq.  
 165 (5):

166

$$167 \quad \delta^{34}\text{S}_{nss} = \delta^{34}\text{S}_{DMS} \times F_{DMS-SO_4} + \delta^{34}\text{S}_{anthropogenic} \times (1 - F_{DMS-SO_4}) \quad (5)$$

168

169 where F represents the fraction (DMS and anthropogenic),  $\delta^{34}\text{S}_{nss}$  represents the  $\delta^{34}\text{S}$  of the sample,  $\delta^{34}\text{S}_{DMS}$   
 170 and  $\delta^{34}\text{S}_{anthropogenic}$  refer to the mean isotopic composition of the end-members (DMS and anthropogenic). The  
 171 DMS end-member was taken from Amrani et al., 2013, with a  $\delta^{34}\text{S}$  composition of +189.87 ± 0.5 ‰. The  
 172 anthropogenic end-member varies by season and is constrained by a combination of literature reports and new  
 173 findings in this study. For samples where air masses originated from the continent (spring, winter), an IGP end-  
 174 member was used. The IGP end-member had a  $\delta^{34}\text{S}$  of 2.3 ± 1.7 ‰ calculated from this study and literature (Dasari  
 175 and Widory, 2024; Sawlani et al., 2019, Table S1). The ship end-member had a  $\delta^{34}\text{S}$  of 3 ± 3 ‰ taken from studies  
 176 that measured  $\delta^{34}\text{-SO}_4$  and  $\delta^{34}\text{-SO}_2$  in the North Atlantic, which is thought to be representative of remote air  
 177 masses with strong ship emissions from heavy fuel oil (Seguin et al., 2010, 2011; Wadleigh, 2004).

178

179

180 **2.6 Satellite imagery and computational analysis**

181 The Hybrid Single-Particle Lagrangian Integrated Trajectory (HYSPLIT) model was used to run 7-day backward  
182 trajectories from the NOAA Air Research Laboratory (available at <http://ready.arl.noaa.gov/HYSPLIT.php>). Back  
183 trajectories for seasonal clusters were calculated for summer (June–September 2015), winter (December–March  
184 2015–2016) and spring (April–May 2015).

185 MERRA-2 (Modern-Era Retrospective Analysis for Research and Applications, version 2) and TROPES  
186 (TROpospheric Ozone and its Precursors from Earth System Sounding) were used to retrieve model-estimated  
187 surface concentrations of black carbon and sulfate. MERRA-2 is a reanalysis product that uses remote sensing  
188 aerosol optical depth (satellite- and ground-based) in combination with the Goddard Earth Observing System  
189 Model, Version 5 to calculate aerosol concentrations (Buchard et al., 2017; Gelaro et al., 2017; Randles et al.,  
190 2017). TROPES includes additional satellite measurements (TES, AIRS, TROPOMI, and OMPS) combined  
191 with a retrieval algorithm to obtain sulfate surface concentrations (Miyazaki, 2024).

192

193 **2.7 Emission inventory**

194 The Community Emissions Data System (CEDSV2021\_04\_21) is a bottom-up emission inventory that provides  
195 gridded and national fluxes of short-lived climate pollutants (Hoesly et al., 2018). The national inventory dataset  
196 is available at <https://zenodo.org/records/4741285>.

## 197 **3 Results and discussion**

### 198 **3.1 Constraints on isotopic signatures of different sources**

199 Reports on the isotopic composition of sulfate from different sources and regions display a large range, although  
200 marine natural sources are clearly enriched in  $^{34}\text{S}$  compared to anthropogenic sources. Natural sources  
201 considered in this study were sea spray and dimethyl sulfide (DMS), the dominant marine biogenic source. Sea  
202 spray and DMS have a well-defined isotopic composition of  $+21 \pm 0.2 \text{ ‰}$  and  $+19.7 \pm 0.5 \text{ ‰}$ , respectively  
203 (Amrani et al., 2013; Böttcher et al., 2007; Rees et al., 1978). In contrast, fossil fuel end-members can vary ( $-35$   
204 to  $+33 \text{ ‰}$ ) depending on fuel type (liquid vs solid), as well as having strong geographical differences  
205 (Jongebloed et al., 2023; Lee et al., 2023). Additional details on sulfate sources and considerations in sulfur-  
206 isotopic attribution studies are provided in the Supplementary Information (Text S1).

207 To account for the potential variability in fossil fuel isotope end-members, an anthropogenic end-member was  
208 determined through sampling in the regional source-integrating air masses of the IGP, with end-member  
209 uncertainty accounted for through error propagation (see Method S2). The samples were first split based on air  
210 mass origin into a continental anthropogenic end-member and an oceanic anthropogenic end-member. The  
211 oceanic anthropogenic input was expected to be predominantly from ship emissions, with a  $\delta^{34}\text{S}$  signature of  $3 \pm$   
212  $3 \text{ ‰}$  taken from the literature on the marine anthropogenic end-member (Seguin et al., 2010, 2011; Wadleigh,  
213 2004, Text S1). The oceanic anthropogenic and continental anthropogenic end-members were treated as distinct  
214 to reflect their different origins. Ship emissions may contribute to the continental end-member, but available  
215 top-down (MERRA-2) and bottom-up (CEDS) constraints indicate that these contributions are much smaller  
216 than land-based continental emissions (Buchard et al., 2017; Randles et al., 2017; Hoesly et al., 2018). In any  
217 case, the choice of end-member changes the inferred anthropogenic contribution by at most  $\sim 3\%$ .

218 The integrated continental anthropogenic signature was calculated directly from  $\delta^{34}\text{S}(\text{SO}_4^{2-})$  measured on  
219 aerosol filters in the IGP (Delhi and BCOB), with samples measured in this study and from the literature,  
220 resulting in an end-member value of  $2.3 \pm 1.7 \text{ ‰}$  (see Fig. 2, Table S1; Dasari & Widory, 2024; Sawlani et al.,  
221 2019, n = 50).~~The integrated continental anthropogenic signature was calculated from the IGP samples in this~~  
222 ~~study and from the literature, resulting in an end-member value of  $2.3 \pm 1.7 \text{ ‰}$ .~~(see Fig. 2, Table S1; Dasari &  
223 Widory, 2024; Sawlani et al., 2019, n = 50)–Analysing source aerosols captures isotope fractionation during  
224  $\text{SO}_2$  oxidation to sulfate, which can be substantial ( $\approx 3\%$  enrichment in urban environments, See SI Text S1; Lee  
225 et al., 2023). The IGP end-member in this study was assumed to be predominantly anthropogenic. Potential  
226 crustal and biogenic contributions are expected to be minor (Dasari & Widory, 2024). Our sensitivity analysis  
227 shows that including a 5–10% non-anthropogenic sulfate fraction does not change the source apportionment  
228 beyond the propagated uncertainty (see SI Text S3). We also investigated the use of a Keeling plot to determine  
229 the anthropogenic end-member, but did not apply this approach because mixed and variable sources could bias  
230 the inferred end-member toward depleted values (see SI Text 3 and SI Fig. 3). Anthropogenic sulfate also  
231 includes minor contributions from crustal and biomass burning sources, which have not been separated in this  
232 study. The average from this study was slightly lower due to one sample showing a near-zero  $\delta^{34}\text{S}$  value ( $-0.07$   
233  $\text{ ‰}$ ). This  $\delta^{34}\text{S}$ -depleted sample likely reflects sulfate formation through oxidation catalyzed by transition metal  
234 ions (TMI) and is associated with poor air quality, reported during hazy conditions (Harris et al., 2013; Sawlani  
235 et al., 2019). Alternatively, this type of isotope depletion has been proposed to be related to increased coal input

236 or terrigenous sulfate (Dasari and Widory, 2024). These depleted oxidative pathways/sources are likely to occur  
237 as a continuum, motivating the inclusion of the depleted sample.

238

### 239 **3.2 Abundance of sulfate aerosols over the northern Indian Ocean**

240 There are only limited reports of measured sulfate concentrations over the Indian Ocean, an area integral to South  
241 Asia's monsoon/hydrological cycles and aerosol-affected regional climate forcing. This reduces the confidence in  
242 our understanding of the regional loadings of sulfate and the effective regional climate forcing. The loadings for  
243 the non-sea salt sulfate (nss-SO<sub>4</sub><sup>2-</sup>) over the northern Indian Ocean for winter, spring, and summer in this study  
244 were  $10 \pm 4 \mu\text{g m}^{-3}$  ( $96 \pm 6 \%$  nss-SO<sub>4</sub><sup>2-</sup>, full period  $n = 43$  from Dasari et al., 2019),  $5.5 \pm 1 \mu\text{g m}^{-3}$  ( $98.5 \pm 0.1 \%$   
245 nss-SO<sub>4</sub><sup>2-</sup>),  $1 \pm 0.2 \mu\text{g m}^{-3}$  ( $85.5 \pm 5.5 \%$  nss-SO<sub>4</sub><sup>2-</sup>), respectively, with these values broadly agreeing with previous  
246 reports from the MCOH receptor of the South Asian outflow (Budhavant et al., 2023, 2024b).

247 Seasonal differences are due to both fluctuating emissions and varying seasonal air transport from the source  
248 regions (Fig. 1). These meteorological factors (wind speed, boundary layer height, humidity, etc.) cause winter  
249 conditions to be favorable for long-range aerosol transport from the polluted IGP out over the northern Indian  
250 Ocean (Aswini et al., 2020; Dasari et al., 2019; Kesti et al., 2020; Ram et al., 2012). With a shortage of in situ  
251 measurements, estimates from remote sensing provide a picture of sulfate loadings for remote regions; expansion  
252 of in situ atmospheric observatory measurements is critical to the validation of the accuracy of derived estimates  
253 from remote sensing.

254 Remote sensing estimations of sulfate loadings are commonly derived from optical measurements of columnar  
255 data, which can differ greatly from ground conditions. The indirect estimates of sulfate surface loadings from  
256 remote sensing (MERRA-2, TROPES at  $p = 1000$  hPa) were 2-5 times lower than the in situ sulfate measurements  
257 in this study (see Fig. S1). These discrepancies need to be confirmed by forthcoming longer and more complete  
258 in situ measurement records of sulfate in this critical region for sulfate-climate effects. Long-term in situ records  
259 remain pivotal in understanding long-term changes, which become even more valuable when combined with  
260 additional analysis such as isotopic source apportionment.

261

### 262 **3.3 Source-diagnostic isotopic composition of sulfate aerosols over the northern Indian Ocean**

263 Refined constraints on sulfate sources improve our understanding of the atmospheric cycle of climate-forcing  
264 anthropogenic sulfate over South Asia. The study results show that anthropogenic sulfate dominated in the South  
265 Asian outflow intercepted over the northern Indian Ocean, yet there is also substantial input of natural sulfate,  
266 especially in the monsoon period. The input of anthropogenic sources to the nss-SO<sub>4</sub><sup>2-</sup> loading was  $934 \pm 144 \%$ ,  
267  $878 \pm 109 \%$ ,  $667 \pm 123 \%$  for winter, spring (pre-monsoon), and summer (monsoon), respectively (Fig. 2; Table  
268 S1).

269 These fractions translate into anthropogenic sulfate concentrations of  $0.6 \pm 0.2 \mu\text{g m}^{-3}$  (summer),  $4.86 \pm 0.87 \mu\text{g m}^{-3}$  (spring), and  $89.49 \pm 5 \mu\text{g m}^{-3}$  (samples with  $\delta^{34}\text{S}$ ; winter). Although the summer conditions are cleanest, the region is still highly affected by anthropogenic input, with freight ships during that time likely being an important source. Three major shipping lanes cross the northern Indian Ocean. During the study period, the global shipping emissions were nearly equal to the cumulative emissions of South Asia (McDuffie et al., 2020). These loadings are elevated given the remote location, even with respect to health guidelines for exposure to fine particulate matter.

276 The World Health Organization (WHO) annual guideline for  $\text{PM}_{2.5}$  is  $5 \mu\text{g m}^{-3}$  (World Health Organization, 2021), a limit which is frequently exceeded in both winter and spring even this far out over the Indian Ocean, despite local emissions being documented to be low (Budhavant et al., 2015). It is worth noting that a portion of the sulfate loading in the winter air masses from the Bay of Bengal may possibly be influenced by input from mangroves, which emit hydrogen sulfide ( $\text{H}_2\text{S}$ ). This gas is rapidly oxidized and typically has a  $\delta^{34}\text{S}$  below 0 ‰ (Jamieson & Wadleigh, 1999). The  $\text{H}_2\text{S}$  flux from mangroves is potentially significant with emissions estimates ranging from approximately 10 – 25 % of South Asia’s anthropogenic emissions (Ganguly et al., 2018; Hoesly et al., 2018). However, analysis of the back trajectories suggests that sulfate loadings were influenced more by seasonal variation than by specific trajectory pathways (see Fig. S2). Sulfate loadings reaching MCOH are elevated and are attributed primarily to anthropogenic sources.

286 This isotope-based source apportionment of sulfate in the receptor-integrated South Asian outflow appears broadly consistent with other regional studies. A study over the northern Bay of Bengal reported  $\delta^{34}\text{S} = 4.5 \pm 1.3\text{‰}$  in  $\text{PM}_{10}$  during February–April 2013 (Rastogi et al., 2020). Applying our  $\delta^{34}\text{S}$  two-end-member mixing model to those Port Blair  $\text{PM}_{10}$  values indicates that at least ~90% of sulfate was anthropogenic. This should be viewed as a conservative lower bound because the sea-salt contribution for the isotopic data was not reported (so no sea-salt correction could be applied), and  $\text{PM}_{10}$  generally contains a larger sea-salt fraction. Similarly, the ICARB-2018 ship campaign estimated anthropogenic sulfate to make up 96 % of the  $\text{nss-SO}_4^{2-}$  in the Arabian Sea and Indian Ocean (Aswini et al., 2020), using the ratio of methanesulfonic acid (MSA)/ $\text{nss-SO}_4^{2-}$ . These results suggest a quite limited influence of DMS on the total sulfate mass balance over the northern Indian Ocean, even though globally DMS emissions are expected to be a quarter the size of anthropogenic emissions (Lana et al., 2011). These results provide quantitative constraints on sources, showing a strong dominance of anthropogenic sources of sulfate in the northern Indian Ocean, yet with seasonal variations.

298

### 299 **3.4 Relationships between sulfate and black carbon**

300 Sulfate precursors and black carbon (BC) are both emitted in large quantities from fossil fuel combustion, yet they also have other separate sources. We explored the extent of co-emission of these two short-lived climate pollutants (SLCPs), having opposing signs in their climate forcing. By comparing isotope-based source indicators ( $\delta^{34}\text{S}$ – $\text{SO}_4$  and  $\Delta^{14}\text{C}$ –BC), we observe a positive correlation ( $r^2 = 0.759$ ,  $p \ll 0.05$ ,  $n = 7$ ) between anthropogenic sulfate and the fraction of BC attributed to fossil fuel combustion for the outflow receptor observatory at MCOH (winter and spring) (see Fig. 3 inset). Samples from BCOB, which were used to represent the anthropogenic end-member of sulfate, were assumed to be predominantly anthropogenic in origin (~100 %), although minor contributions from dust and biomass are expected (Dasari and Widory, 2024). Summer data were too limited for robust conclusions,

308 although a similar pattern was observed, potentially reflecting differences in emission sources (see Fig. S3). The  
309 positive correlation between the isotope fingerprints of these SLCPs lends further credence to the  $\delta^{34}\text{S}$ -based  
310 findings that fossil fuel combustion is indeed a major source of  $\text{SO}_4^{2-}$  over South Asia, with additional insight  
311 provided by examining the relationship between  $\text{SO}_4^{2-}$  and climate-warming BC.

312 Black carbon and sulfate, in part co-emitted, have opposite climatic effects, with BC enhancing climate warming  
313 while sulfate masks climate warming. Their opposing climatic effects lead to large uncertainties in radiative  
314 forcing due to the ratio of scattering vs absorbing vectors, especially in regions with high loadings of both BC and  
315  $\text{SO}_4^{2-}$ , such as South Asia (Li et al., 2022). The BC/ $\text{SO}_4^{2-}$  ratio for the study period was  $0.075 \pm 0.03$  (spring and  
316 winter; summer was excluded due to high variability). The BC/ $\text{SO}_4^{2-}$  ratio in the surface layer estimated from  
317 remote sensing by MERRA-2 was much higher for winter during which it was predicted to be 0.16 (2016) and for  
318 spring (April 2013) during which it was predicted to be 0.15; both were twice overestimated compared to our  
319 direct in situ measurements. The observed BC/ $\text{SO}_4^{2-}$  ratio was compared with an inventory-based BC/ $\text{SO}_2$  ratio  
320 from the Community Emissions Data System (CEDS v2021-04-21). The BC/ $\text{SO}_2$  ratio was obtained by  
321 aggregating BC and  $\text{SO}_2$  fluxes over India, Pakistan, and Bangladesh. As inventories report  $\text{SO}_2$  (not sulfate),  
322 BC/ $\text{SO}_2$  is used as a proxy for BC/ $\text{SO}_4^{2-}$ . The ratio from CEDS was 0.097 (2015-2019 average; Hoesly et al.,  
323 2018), which is close to the BC/ $\text{SO}_4^{2-}$  ratio of  $0.075 \pm 0.03$  constrained by in situ measurements in the current  
324 study, ~~with MERRA 2 being higher.~~ When we instead compare to the in situ anthropogenic sulfate fraction  
325 (BC/anthro- $\text{SO}_4^{2-}$ ), the agreement improves ( $0.082 \pm 0.03$ ; spring and winter). The uncertainty reflects  
326 measurement variability only and does not include additional uncertainty propagated from the  $\delta^{34}\text{S}$  end-member  
327 constraints. Deviation between emission inventory and in-situ may reflect the unaccounted biogenic sulfur inputs  
328 (lowering BC/ $\text{SO}_4^{2-}$ ), while preferential removal of hygroscopic sulfate during transport would act in the opposite  
329 direction by increasing BC/ $\text{SO}_4^{2-}$  (e.g., Budhavant et al., 2020). There is a need for increased comparison of  
330 BC/ $\text{SO}_4^{2-}$  (and their sources) simulated by models and predicted by emission inventories with greater datasets of  
331 in situ observations in South Asia, given the expected changes in their respective emissions and that reduced  $\text{SO}_4^{2-}$   
332 emissions will unmask current climate warming for the region.

333

334 **4 Conclusion and outlook**

335 There are very large sulfate loadings over South Asia compared with the global average. However, there is poor  
336 spatial coverage of actual measurements of both  $\text{SO}_4^{2-}$  and its source-diagnostic isotopic composition. This study  
337 provides the first multi-seasonal isotope-based source apportionment of sulfate for the integrated outflow airshed  
338 of South Asia. The quantitative results show that anthropogenic nss-sulfate is the major contributor to sulfate  
339 loadings in this region, yet with clear seasonal and spatial variations and with some contributions also from  
340 natural-biogenic sources (e.g., from marine plankton and possibly from mangroves). Quantitative isotope-based  
341 observational constraints on the relative contributions of different sources to atmospheric sulfate are vital for both  
342 understanding total emissions of this important climate forcer and for guiding strategies to mitigate the  
343 anthropogenic components.

344 Future investigations should aim to constrain the long-term trend (decades) of wintertime and summer sources of  
345 sulfate to the South Asian airshed. This will improve the understanding of emission patterns from the heavily  
346 polluted IGP, as well as provide potential insights into atmospheric processing due to South Asia's changing  
347 meteorology. Aerosol loadings have already been shown to strongly affect the monsoon period (Krishnan et al.,  
348 2016; Ramarao et al., 2023). Moreover, both current and past emissions will be needed to understand future  
349 changes, with emissions expected to decrease due to socio-economic pressures. Thus, there is an urgent need for  
350 improved understanding of all facets of sulfate aerosols to help improve resilience against future climatic impacts,  
351 including the extent to which we may need to anticipate enhanced warming (with South Asia being particularly  
352 sensitive to heat extremes) due to the demasking of climate warming caused by decreasing sulfate loadings.

353 **Additional information**

354 Additional information can be found in the attached Supplementary Information. Data are available in the Bolin  
355 Centre Database (DOI: 10.17043/clarke-2025-v3m0nk-1).

356

357 **Author contributions**

358 This study was conceptualized by Ö.G. and H.H. Atmospheric sampling strategies and campaign execution were  
359 realized by K.B., H.H. and Ö.G. Laboratory procedures, data quality assessments and calculations were  
360 performed by M.R., S.C., H.H., K.R. and E.K. Interpretations and the first draft of the manuscript were  
361 primarily contributed by H.H., Ö.G., S.C. Finally, S.C. produced all display items and wrote the manuscript  
362 with all authors contributing to detailed data interpretation and writing.

363

364 **Acknowledgements**

365 Elena Kirillova and Srinivas Bikkina (Stockholm University) are acknowledged for their support during the  
366 field campaigns. We thank the technical staff at the BCOB and MCOH for their continued field support. Special  
367 thanks are due to the Maldives Meteorological Service and the government of the Republic of Maldives for their  
368 ongoing support of the joint MCOH operation. Krishnakant Budhavant expresses thanks for the additional  
369 support from the Regional Resource Centre for Asia and the Pacific (RRC.AP) at the Asian Institute of  
370 Technology (AIT), Thailand. This is Vegacenter publication number [to be assigned after the paper accepted].

371

372 The authors acknowledge the use of the ChatGPT large-language model (OpenAI) for grammar and language  
373 editing assistance; all scientific content and interpretations are the authors' own.

374

375 **Financial support**

376 This research was funded by the Swedish Research Council (VR Grant 2017-01601 to ÖG), the Swedish  
377 Research Council for Sustainable Development (FORMAS Grant 2023-01234 to Ö.G.). We also acknowledge  
378 the Swedish Research Council (VR) for financial support to the NordSIMS-Vegacenter national research  
379 infrastructure (Grant 2017-00671).

380

381 **Competing interests**

382 The authors declare that they have no conflict of interest.

383

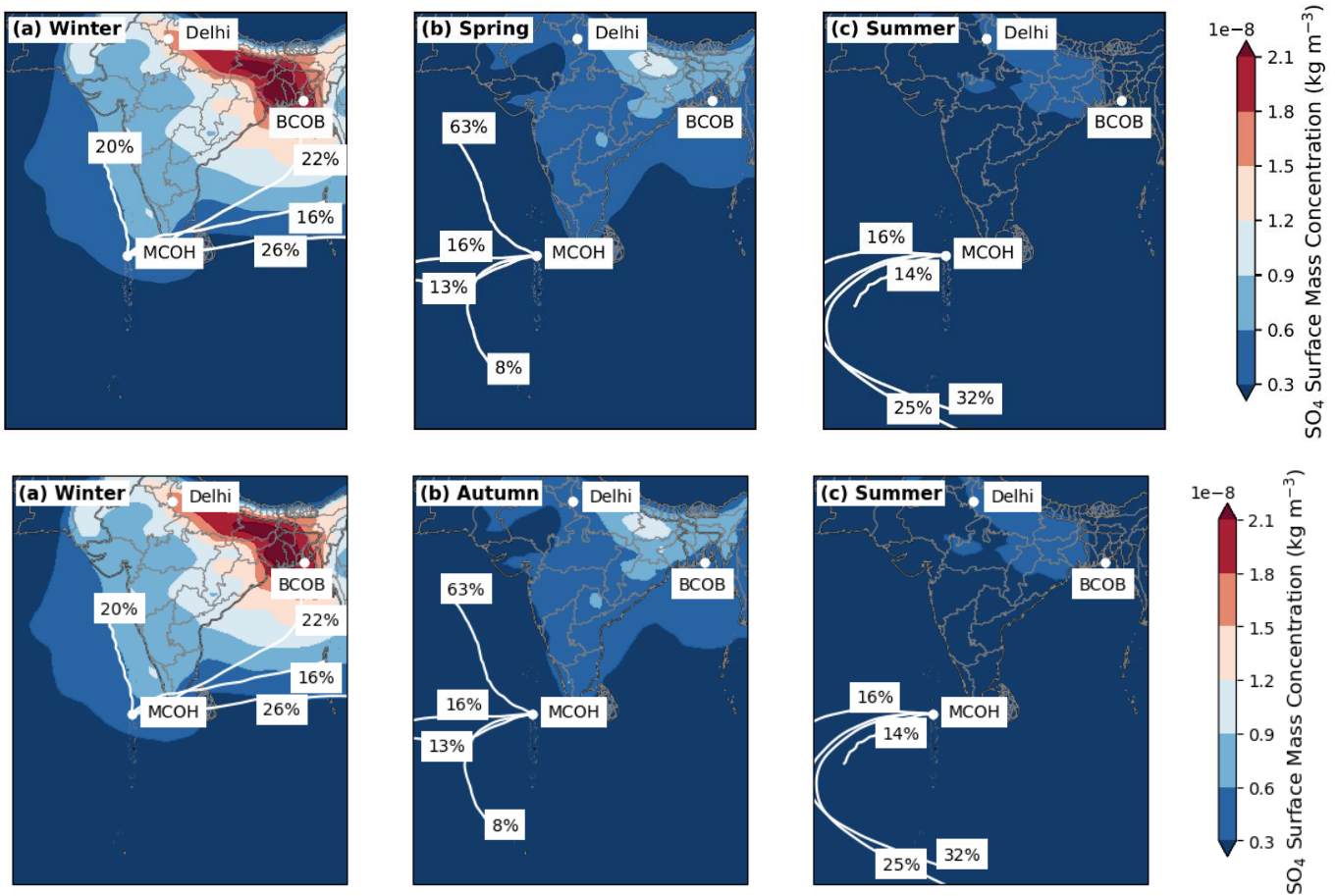
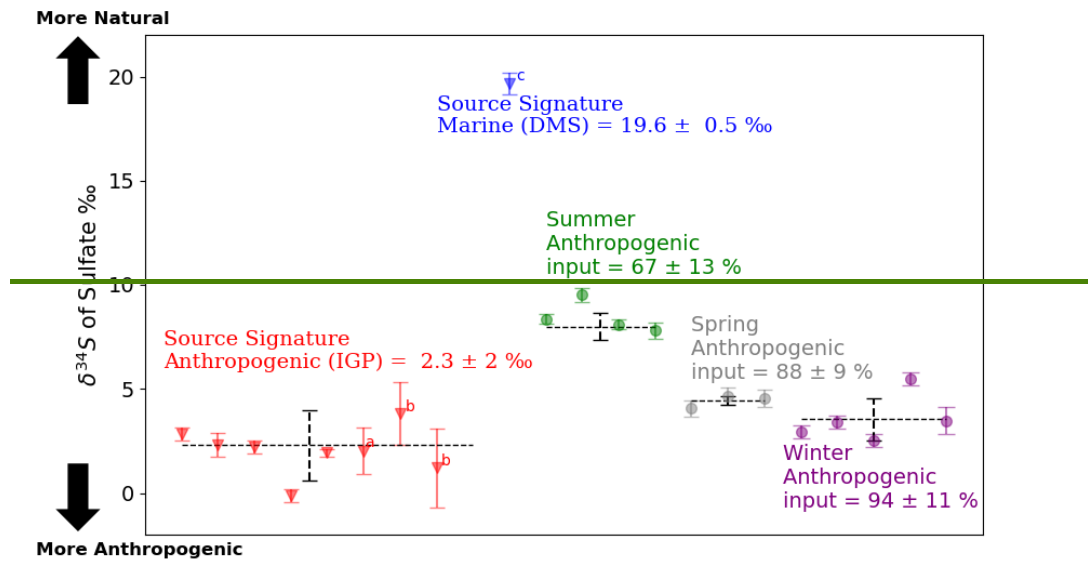
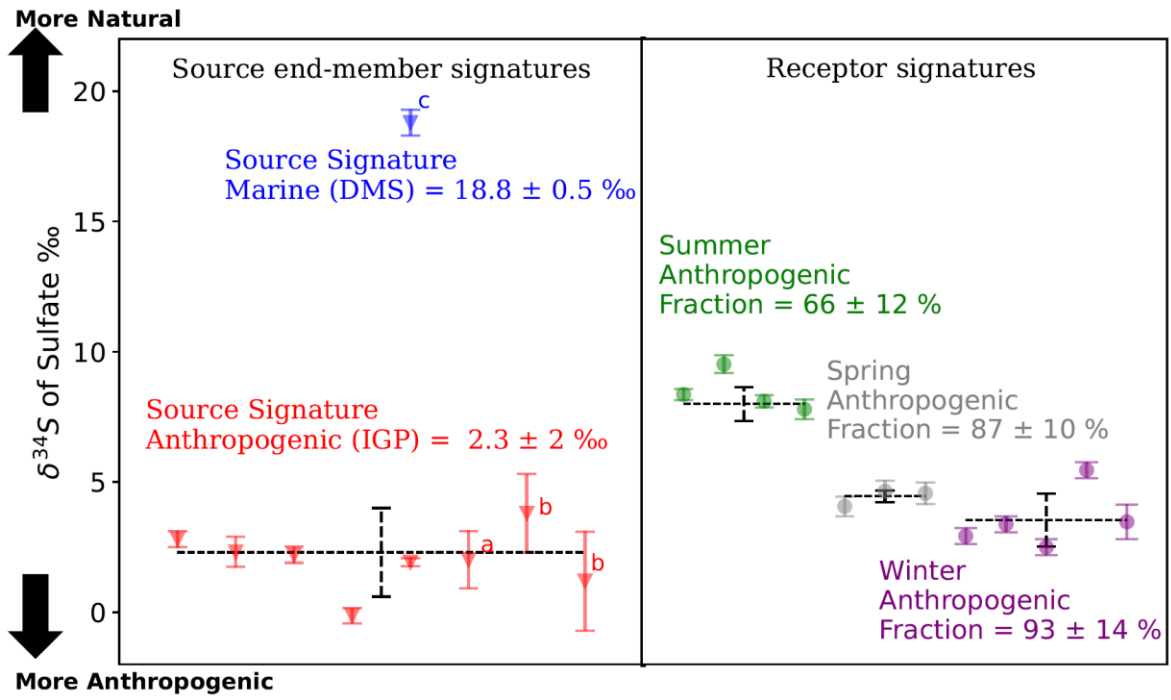


*Fig. 1. Remote sensing estimates of sulfate surface concentration (MERRA-2) and average back trajectories (7-day clusters; HYSPLIT, white lines depict the mean paths of the HYSPLIT back-trajectory clusters) for South Asia, for three seasons: (a) winter (December–March 2015–2016); (b) spring (April–May 2013); (c) summer (June–September 2015).*



388



389

390

391

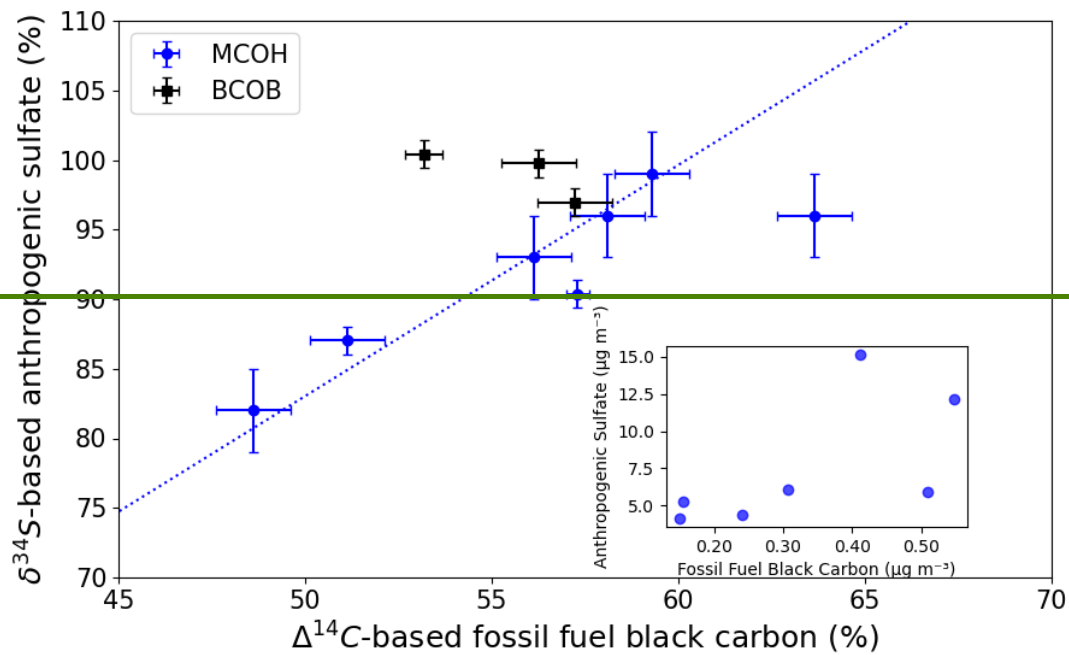
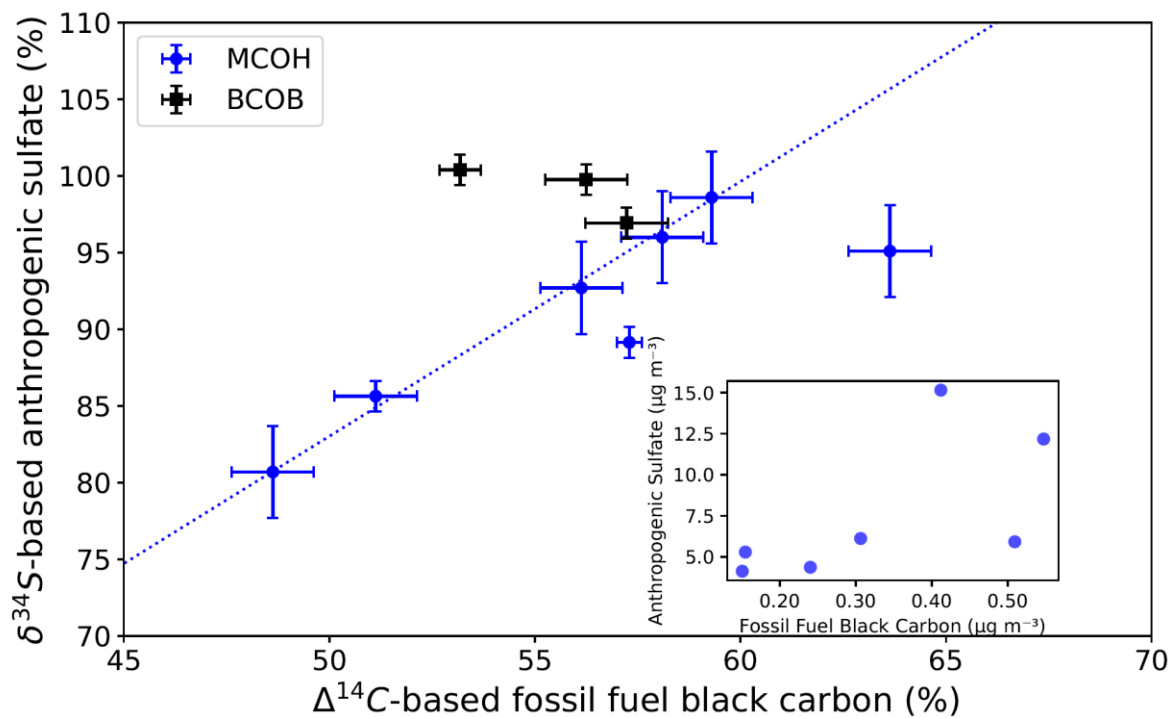
392

393

394

Fig. 2. Sulfate  $\delta^{34}\text{S}$  composition for MCOH and end-members: IGP source signature (this study,  $n = 5$ ;  $a = \text{Dasari \& Widory, 2024, } n = 15$ ;  $b = \text{Sawlani et al., 2019, } n = 30$ ), DMS source signature (blue;  $c = \text{Amrani et al., 2013, } n = 16$ ). MCOH summer (green), spring (grey), and winter (purple). Error bars for this study's samples show  $\pm 4\sigma$  (instrumental analytical precision, per measurement). Literature points and seasonal aggregates show  $\pm 2\sigma$  (between-sample standard deviation).

395



398 **Fig. 3.** Relationships between fossil fuel black carbon and anthropogenic sulfate for MCOH (spring,  
 399 summer; blue circles) and BCOB (black squares), calculated using isotopic composition ( $\Delta^{14}\text{C}$ ,  $\delta^{34}\text{S}$ ).  
 400 The inset graph shows the actual concentrations of fossil fuel black carbon and anthropogenic sulfate  
 401 for MCOH.

402

403

404

405 **References**

- 406 Aas, W., Mortier, A., Bowersox, V., Cherian, R., Faluvegi, G., Fagerli, H., Hand, J., Klimont, Z.,  
407 Galy-Lacaux, C., Lehmann, C. M. B., Myhre, C. L., Myhre, G., Olivié, D., Sato, K., Quaas, J., Rao, P.  
408 S. P., Schulz, M., Shindell, D., Skeie, R. B., Stein, A., Takemura, T., Tsyro, S., Vet, R., and Xu, X.:  
409 Global and regional trends of atmospheric sulfur, *Sci. Rep.*, 9, [https://doi.org/10.1038/s41598-018-](https://doi.org/10.1038/s41598-018-37304-0)  
410 37304-0, 2019.
- 411 Amrani, A., Said-Ahmad, W., Shaked, Y., and Kiene, R. P.: Sulfur isotope homogeneity of oceanic  
412 DMSP and DMS, *Proc. Natl. Acad. Sci. U. S. A.*, 110, <https://doi.org/10.1073/pnas.1312956110>,  
413 2013.
- 414 Andersson, A., Deng, J., Du, K., Zheng, M., Yan, C., Sköld, M., and Gustafsson, Ö.: Regionally-  
415 varying combustion sources of the January 2013 severe haze events over eastern China, *Environ. Sci.*  
416 *Technol.*, 49, <https://doi.org/10.1021/es503855e>, 2015.
- 417 Aswini, A. R., Hegde, P., Aryasree, S., Girach, I. A., and Nair, P. R.: Continental outflow of  
418 anthropogenic aerosols over Arabian Sea and Indian Ocean during wintertime: ICARB-2018  
419 campaign, *Science of the Total Environment*, 712, <https://doi.org/10.1016/j.scitotenv.2019.135214>,  
420 2020.
- 421 Berresheim, H., Elste, T., Tremmel, H. G., Allen, A. G., Hansson, H. C., Rosman, K., Dal Maso, M.,  
422 Mäkelä, J. M., Kulmala, M., and O'Dowd, C. D.: Gas-aerosol relationships of H<sub>2</sub>SO<sub>4</sub>, MSA, and OH:  
423 Observations in the coastal marine boundary layer at Mace Head, Ireland, *Journal of Geophysical*  
424 *Research Atmospheres*, 107, <https://doi.org/10.1029/2000JD000229>, 2002.
- 425 Bikkina, S., Andersson, A., Kirillova, E. N., Holmstrand, H., Tiwari, S., Srivastava, A. K., Bisht, D.  
426 S., and Gustafsson, Ö.: Air quality in megacity Delhi affected by countryside biomass burning, *Nat.*  
427 *Sustain.*, 2, <https://doi.org/10.1038/s41893-019-0219-0>, 2019.
- 428 Böttcher, M. E., Brumsack, H. J., and Dürselen, C. D.: The isotopic composition of modern seawater  
429 sulfate: I. Coastal waters with special regard to the North Sea, *Journal of Marine Systems*, 67,  
430 <https://doi.org/10.1016/j.jmarsys.2006.09.006>, 2007.
- 431 Buchard, V., Randles, C. A., da Silva, A. M., Darmenov, A., Colarco, P. R., Govindaraju, R., Ferrare,  
432 R., Hair, J., Beyersdorf, A. J., Ziemba, L. D., and Yu, H.: The MERRA-2 aerosol reanalysis, 1980  
433 onward. Part II: Evaluation and case studies, *J. Clim.*, 30, <https://doi.org/10.1175/JCLI-D-16-0613.1>,  
434 2017.
- 435 Budhavant, K., Andersson, A., Bosch, C., Kruså, M., Murthaza, A., Zahid, and Gustafsson, Ö.:  
436 Apportioned contributions of PM<sub>2.5</sub> fine aerosol particles over the Maldives (northern Indian Ocean)  
437 from local sources vs long-range transport, *Science of the Total Environment*, 536,  
438 <https://doi.org/10.1016/j.scitotenv.2015.07.059>, 2015.
- 439 Budhavant, K., Andersson, A., Holmstrand, H., Bikkina, P., Bikkina, S., Satheesh, S. K., and  
440 Gustafsson, Ö.: Enhanced Light-Absorption of Black Carbon in Rainwater Compared With Aerosols  
441 Over the Northern Indian Ocean, *Journal of Geophysical Research: Atmospheres*, 125,  
442 <https://doi.org/10.1029/2019JD031246>, 2020.
- 443 Budhavant, K., Andersson, A., Holmstrand, H., Satheesh, S. K., and Gustafsson, Ö.: Black carbon  
444 aerosols over Indian Ocean have unique source fingerprint and optical characteristics during monsoon  
445 season, *Proc. Natl. Acad. Sci. U. S. A.*, 120, <https://doi.org/10.1073/pnas.2210005120>, 2023.
- 446 Budhavant, K., Manoj, M. R., Nair, H. R. C. R., Gaita, S. M., Holmstrand, H., Salam, A., Muslim, A.,  
447 Satheesh, S. K., and Gustafsson, Ö.: Changing optical properties of black carbon and brown carbon

448 aerosols during long-range transport from the Indo-Gangetic Plain to the equatorial Indian Ocean,  
449 *Atmos. Chem. Phys.*, 24, 11911–11925, <https://doi.org/10.5194/acp-24-11911-2024>, 2024a.

450 Budhavant, K., Manoj, M. R., Nair, H. R. C. R., Gaita, S. M., Holmstrand, H., Salam, A., Muslim, A.,  
451 Satheesh, S. K., and Gustafsson, Ö.: Changing optical properties of black carbon and brown carbon  
452 aerosols during long-range transport from the Indo-Gangetic Plain to the equatorial Indian Ocean,  
453 *Atmos. Chem. Phys.*, 24, 11911–11925, <https://doi.org/10.5194/acp-24-11911-2024>, 2024b.

454 Charlson, R. J., Langner, J., Rodhe, H., Leovy, C. B., and Warren, S. G.: Perturbation of the Northern  
455 Hemisphere radiative balance by backscattering from anthropogenic sulfate aerosols, *Tellus, Series A-*  
456 *B*, 43 A-B, <https://doi.org/10.3402/tellusb.v43i4.15404>, 1991.

457 Chen, B., Andersson, A., Lee, M., Kirillova, E. N., Xiao, Q., Kruså, M., Shi, M., Hu, K., Lu, Z.,  
458 Streets, D. G., Du, K., and Gustafsson, Ö.: Source forensics of black carbon aerosols from China,  
459 *Environ. Sci. Technol.*, 47, <https://doi.org/10.1021/es401599r>, 2013.

460 Dasari, S. and Widory, D.: Retrospective Isotopic Analysis of Summertime Urban Atmospheric  
461 Sulfate in South Asia Using Improved Source Constraints, *ACS ES&T Air*, 1, 357–364,  
462 <https://doi.org/10.1021/acsestair.3c00060>, 2024.

463 Dasari, S., Andersson, A., Bikkina, S., Holmstrand, H., Budhavant, K., Satheesh, S., Asmi, E., Kesti,  
464 J., Backman, J., Salam, A., Bisht, D. S., Tiwari, S., Hameed, Z., and Gustafsson, Ö.: Photochemical  
465 degradation affects the light absorption of water-soluble brown carbon in the South Asian outflow,  
466 *Sci. Adv.*, 5, <https://doi.org/10.1126/sciadv.aau8066>, 2019.

467 Dasari, S., Andersson, A., Stohl, A., Evangeliou, N., Holmstrand, H., Budhavant, K., Salam, A., and  
468 Gustafsson, Ö.: Source Quantification of South Asian Black Carbon Aerosols with Isotopes and  
469 Modeling, *Environ. Sci. Technol.*, 54, 11771–11779, <https://doi.org/10.1021/acs.est.0c02193>, 2020.

470 Elguindi, N., Granier, C., Stavrou, T., Darras, S., Bauwens, M., Cao, H., Chen, C., Denier van der  
471 Gon, H. A. C., Dubovik, O., Fu, T. M., Henze, D. K., Jiang, Z., Keita, S., Kuenen, J. J. P., Kurokawa,  
472 J., Liousse, C., Miyazaki, K., Müller, J. F., Qu, Z., Solmon, F., and Zheng, B.: Intercomparison of  
473 Magnitudes and Trends in Anthropogenic Surface Emissions From Bottom-Up Inventories, Top-  
474 Down Estimates, and Emission Scenarios, *Earths Future*, 8, <https://doi.org/10.1029/2020EF001520>,  
475 2020.

476 Ganguly, D., Ray, R., Majumdar, N., Chowdhury, C., and Jana, T. K.: Biogenic hydrogen sulphide  
477 emissions and non-sea sulfate aerosols over the Indian Sundarban mangrove forest, *J. Atmos. Chem.*,  
478 75, 319–333, <https://doi.org/10.1007/s10874-018-9382-3>, 2018.

479 Gelaro, R., McCarty, W., Suárez, M. J., Todling, R., Molod, A., Takacs, L., Randles, C. A.,  
480 Darmenov, A., Bosilovich, M. G., Reichle, R., Wargan, K., Coy, L., Cullather, R., Draper, C., Akella,  
481 S., Buchard, V., Conaty, A., da Silva, A. M., Gu, W., Kim, G. K., Koster, R., Lucchesi, R., Merkova,  
482 D., Nielsen, J. E., Partyka, G., Pawson, S., Putman, W., Rienecker, M., Schubert, S. D., Sienkiewicz,  
483 M., and Zhao, B.: The modern-era retrospective analysis for research and applications, version 2  
484 (MERRA-2), *J. Clim.*, 30, <https://doi.org/10.1175/JCLI-D-16-0758.1>, 2017.

485 Gupta, G., Ratnam, M. V., and Madhavan, B. L.: Changing patterns in the highly contributing aerosol  
486 types/species across the globe in the past two decades, *Science of the Total Environment*, 897,  
487 <https://doi.org/10.1016/j.scitotenv.2023.165389>, 2023.

488 Harris, E., Sinha, B., Van Pinxteren, D., Tilgner, A., Fomba, K. W., Schneider, J., Roth, A., Gnauk,  
489 T., Fahlbusch, B., Mertes, S., Lee, T., Collett, J., Foley, S., Borrmann, S., Hoppe, P., and Herrmann,  
490 H.: Enhanced role of transition metal ion catalysis during in-cloud oxidation of SO<sub>2</sub>, *Science (1979)*,  
491 340, <https://doi.org/10.1126/science.1230911>, 2013.

492 Hoesly, R. M., Smith, S. J., Feng, L., Klimont, Z., Janssens-Maenhout, G., Pitkanen, T., Seibert, J. J.,  
493 Vu, L., Andres, R. J., Bolt, R. M., Bond, T. C., Dawidowski, L., Kholod, N., Kurokawa, J. I., Li, M.,  
494 Liu, L., Lu, Z., Moura, M. C. P., O'Rourke, P. R., and Zhang, Q.: Historical (1750-2014)  
495 anthropogenic emissions of reactive gases and aerosols from the Community Emissions Data System  
496 (CEDS), *Geosci. Model Dev.*, 11, 369–408, <https://doi.org/10.5194/gmd-11-369-2018>, 2018.

497 Jamieson, R. E. and Wadleigh, M. A.: A study of the oxygen isotopic composition of precipitation  
498 sulphate in eastern Newfoundland, *Water Air Soil Pollut.*, 110,  
499 <https://doi.org/10.1023/a:1005002026009>, 1999.

500 Jongebloed, U. A., Schauer, A. J., Hattori, S., Cole-Dai, J., Larrick, C. G., Salimi, S., Edouard, S. R.,  
501 Geng, L., and Alexander, B.: Sulfur isotopes quantify the impact of anthropogenic activities on  
502 industrial-era Arctic sulfate in a Greenland ice core, *Environmental Research Letters*, 18,  
503 <https://doi.org/10.1088/1748-9326/acdc3d>, 2023.

504 Keene, W. C., Pszenny, A. A. P., Galloway, J. N., and Hawley, M. E.: Sea-salt corrections and  
505 interpretation of constituent ratios in marine precipitation, *Journal of Geophysical Research:*  
506 *Atmospheres*, 91, 6647–6658, <https://doi.org/10.1029/jd091id06p06647>, 1986.

507 Kesti, J., Asmi, E., O'Connor, E. J., Backman, J., Budhavant, K., Andersson, A., Dasari, S., Praveen,  
508 P. S., Zahid, H., and Gustafsson, Ö.: Changes in aerosol size distributions over the Indian Ocean  
509 during different meteorological conditions, *Tellus B Chem. Phys. Meteorol.*, 72,  
510 <https://doi.org/10.1080/16000889.2020.1792756>, 2020.

511 Kirillova, E. N., Andersson, A., Sheesley, R. J., Kruså, M., Praveen, P. S., Budhavant, K., Safai, P.  
512 D., Rao, P. S. P., and Gustafsson, Ö.: 13C- And 14C-based study of sources and atmospheric  
513 processing of water-soluble organic carbon (WSOC) in South Asian aerosols, *Journal of Geophysical*  
514 *Research Atmospheres*, 118, <https://doi.org/10.1002/jgrd.50130>, 2013.

515 Kirillova, E. N., Andersson, A., Tiwari, S., Srivastava, A. K., Bisht, D. S., and Gustafsson, Ö.: Water-  
516 soluble organic carbon aerosols during a full New Delhi winter: Isotope-based source apportionment  
517 and optical properties, *J. Geophys. Res.*, 119, <https://doi.org/10.1002/2013JD020041>, 2014.

518 Krishnan, R., Sabin, T. P., Vellore, R., Mujumdar, M., Sanjay, J., Goswami, B. N., Hourdin, F.,  
519 Dufresne, J. L., and Terray, P.: Deciphering the desiccation trend of the South Asian monsoon  
520 hydroclimate in a warming world, *Clim. Dyn.*, 47, 1007–1027, [https://doi.org/10.1007/s00382-015-](https://doi.org/10.1007/s00382-015-2886-5)  
521 [2886-5](https://doi.org/10.1007/s00382-015-2886-5), 2016.

522 Lana, A., Bell, T. G., Simó, R., Vallina, S. M., Ballabrera-Poy, J., Kettle, A. J., Dachs, J., Bopp, L.,  
523 Saltzman, E. S., Stefels, J., Johnson, J. E., and Liss, P. S.: An updated climatology of surface  
524 dimethylsulfide concentrations and emission fluxes in the global ocean, *Global Biogeochem. Cycles*,  
525 25, <https://doi.org/10.1029/2010GB003850>, 2011.

526 Lee, G., Ahn, J., Park, S. M., Moon, J., Park, R., Sim, M. S., Choi, H., Park, J., and Ahn, J. Y.: Sulfur  
527 isotope-based source apportionment and control mechanisms of PM<sub>2.5</sub> sulfate in Seoul, South Korea  
528 during winter and early spring (2017–2020), *Science of the Total Environment*, 905,  
529 <https://doi.org/10.1016/j.scitotenv.2023.167112>, 2023.

530 Lelieveld, J., Pozzer, A., Pöschl, U., Fnais, M., Haines, A., and Münzel, T.: Loss of life expectancy  
531 from air pollution compared to other risk factors: A worldwide perspective, *Cardiovasc. Res.*, 116,  
532 <https://doi.org/10.1093/cvr/cvaa025>, 2020.

533 Li, C., McLinden, C., Fioletov, V., Krotkov, N., Carn, S., Joiner, J., Streets, D., He, H., Ren, X., Li,  
534 Z., and Dickerson, R. R.: India Is Overtaking China as the World's Largest Emitter of Anthropogenic  
535 Sulfur Dioxide, *Sci. Rep.*, 7, <https://doi.org/10.1038/s41598-017-14639-8>, 2017.

536 Li, J., Carlson, B. E., Yung, Y. L., Lv, D., Hansen, J., Penner, J. E., Liao, H., Ramaswamy, V., Kahn,  
537 R. A., Zhang, P., Dubovik, O., Ding, A., Lacis, A. A., Zhang, L., and Dong, Y.: Scattering and  
538 absorbing aerosols in the climate system, <https://doi.org/10.1038/s43017-022-00296-7>, 1 June 2022.

539 McDuffie, E. E., Smith, S. J., O'Rourke, P., Tibrewal, K., Venkataraman, C., Marais, E. A., Zheng,  
540 B., Crippa, M., Brauer, M., and Martin, R. V.: A global anthropogenic emission inventory of  
541 atmospheric pollutants from sector- And fuel-specific sources (1970-2017): An application of the  
542 Community Emissions Data System (CEDS), *Earth Syst. Sci. Data*, 12, <https://doi.org/10.5194/essd-12-3413-2020>, 2020.

544 Miyazaki, K.: TROPESS Chemical Reanalysis Aerosol SO<sub>4</sub> 6-Hourly 3-Dimensional Product V1,  
545 <https://doi.org/10.5067/TWDAYANXT8UM>, 2024.

546 Nair, H. R. C. R., Budhavant, K., Manoj, M. R., Andersson, A., Satheesh, S. K., Ramanathan, V., and  
547 Gustafsson, Ö.: Aerosol demasking enhances climate warming over South Asia, *NPJ Clim. Atmos.*  
548 *Sci.*, 6, <https://doi.org/10.1038/s41612-023-00367-6>, 2023.

549 Norman, A. L., Barrie, L. A., Toom-Saunty, D., Sirois, A., Krouse, H. R., Li, S. M., and Sharma, S.:  
550 Sources of aerosol sulphate at Alert: Apportionment using stable isotopes, *Journal of Geophysical*  
551 *Research Atmospheres*, 104, <https://doi.org/10.1029/1999JD900078>, 1999.

552 Norman, A. L., Belzer, W., and Barrie, L.: Insights into the biogenic contribution to total sulphate in  
553 aerosol and precipitation in the Fraser Valley afforded by isotopes of sulphur and oxygen, *Journal of*  
554 *Geophysical Research: Atmospheres*, 109, <https://doi.org/10.1029/2002jd003072>, 2004.

555 Ram, K., Sarin, M. M., Sudheer, A. K., and Rengarajan, R.: Carbonaceous and secondary inorganic  
556 aerosols during wintertime fog and haze over urban sites in the Indo-Gangetic plain, *Aerosol Air*  
557 *Qual. Res.*, 12, <https://doi.org/10.4209/aaqr.2011.07.0105>, 2012.

558 Ramanathan, V., Crutzen, P. J., Lelieveld, J., Mitra, A. P., Althausen, D., Anderson, J., Andreae, M.  
559 O., Cantrell, W., Cass, G. R., Chung, C. E., Clarke, A. D., Coakley, J. A., Collins, W. D., Conant, W.  
560 C., Dulac, F., Heintzenberg, J., Heymsfield, A. J., Holben, B., Howell, S., Hudson, J., Jayaraman, A.,  
561 Kiehl, J. T., Krishnamurti, T. N., Lubin, D., McFarquhar, G., Novakov, T., Ogren, J. A., Podgorny, I.  
562 A., Prather, K., Priestley, K., Prospero, J. M., Quinn, P. K., Rajeev, K., Rasch, P., Rupert, S.,  
563 Sadourny, R., Satheesh, S. K., Shaw, G. E., Sheridan, P., and Valero, F. P. J.: Indian Ocean  
564 Experiment: An integrated analysis of the climate forcing and effects of the great Indo-Asian haze,  
565 *Journal of Geophysical Research Atmospheres*, 106, <https://doi.org/10.1029/2001JD900133>, 2001.

566 Ramarao, M. V. S., Ayantika, D. C., Krishnan, R., Sanjay, J., Sabin, T. P., Mujumdar, M., and Singh,  
567 K. K.: Signatures of aerosol-induced decline in evapotranspiration over the Indo-Gangetic Plain  
568 during the recent decades, *Mausam*, 74, 297–310, <https://doi.org/10.54302/mausam.v74i2.6031>, 2023.

569 Randles, C. A., da Silva, A. M., Buchard, V., Colarco, P. R., Darmenov, A., Govindaraju, R.,  
570 Smirnov, A., Holben, B., Ferrare, R., Hair, J., Shinozuka, Y., and Flynn, C. J.: The MERRA-2 aerosol  
571 reanalysis, 1980 onward. Part I: System description and data assimilation evaluation, *J. Clim.*, 30,  
572 <https://doi.org/10.1175/JCLI-D-16-0609.1>, 2017.

573 Rastogi, N., Agnihotri, R., Sawlani, R., Patel, A., Babu, S. S., and Satish, R.: Chemical and isotopic  
574 characteristics of PM<sub>10</sub> over the Bay of Bengal: Effects of continental outflow on a marine  
575 environment, *Science of the Total Environment*, 726, <https://doi.org/10.1016/j.scitotenv.2020.138438>,  
576 2020.

577 Rees, C. E., Jenkins, W. J., and Monster, J.: The sulphur isotopic composition of ocean water  
578 sulphate, *Geochim. Cosmochim. Acta*, 42, [https://doi.org/10.1016/0016-7037\(78\)90268-5](https://doi.org/10.1016/0016-7037(78)90268-5), 1978.

579 Rodiouchkina, K.: Development of a multi-collector inductively coupled plasma massspectrometry  
580 method for measurement of stable sulphur isotope ratios in aerosol sulphate (Dissertation), 2018.

581 Sawlani, R., Agnihotri, R., Sharma, C., Patra, P. K., Dimri, A. P., Ram, K., and Verma, R. L.: The  
582 severe Delhi SMOG of 2016: A case of delayed crop residue burning, coincident firecracker  
583 emissions, and atypical meteorology, *Atmos. Pollut. Res.*, 10,  
584 <https://doi.org/10.1016/j.apr.2018.12.015>, 2019.

585 Seguin, A. M., Norman, A. L., Eaton, S., Wadleigh, M., and Sharma, S.: Elevated biogenic sulphur  
586 dioxide concentrations over the North Atlantic, *Atmos. Environ.*, 44, 1139–1144,  
587 <https://doi.org/10.1016/j.atmosenv.2010.01.005>, 2010.

588 Seguin, A. M., Norman, A. L., Eaton, S., and Wadleigh, M.: Seasonality in size segregated biogenic,  
589 anthropogenic and sea salt sulfate aerosols over the North Atlantic, *Atmos. Environ.*, 45,  
590 <https://doi.org/10.1016/j.atmosenv.2011.09.033>, 2011.

591 Sharma, S. and Kumar, A.: Air pollutant emissions scenario for India - Version 1, The Energy and  
592 Resources Institute, New Delhi, India, 2016.

593 Shenoy, D. M. and Kumar, M. D.: Variability in abundance and fluxes of dimethyl sulphide in the  
594 Indian Ocean, in: *Biogeochemistry*, <https://doi.org/10.1007/s10533-007-9092-4>, 2007.

595 Szopa, S., Naik, V., Adhikary, B., Artaxo, P., Berntsen, T., Collins, W. D., Aas, W., Akritidis, D.,  
596 Allen, R. J., Kanaya, Y., Prather, M. J., Kuo, C., Zhai, P., Pirani, A., Connors, S., Péan, C., Berger, S.,  
597 Caud, N., Chen, Y., Goldfarb, L., Gomis, M., Huang, M., Leitzell, K., Lonnoy, E., Matthews, J.,  
598 Maycock, T., Waterfield, T., Yelekçi, O., Yu, R., and Zhou, B.: Short-lived Climate Forcers  
599 Coordinating Lead Authors: Lead Authors: Contributing Authors: Review Editors: Chapter Scientist:  
600 to the Sixth Assessment Report of the Intergovernmental Panel on Climate Change, 2021.

601 Verma, S., Boucher, O., Shekar Reddy, M., Upadhyaya, H. C., Le Van, P., Binkowski, F. S., and  
602 Sharma, O. P.: Tropospheric distribution of sulphate aerosols mass and number concentration during  
603 INDOEX-IFP and its transport over the Indian Ocean: A GCM study, *Atmos. Chem. Phys.*, 12,  
604 <https://doi.org/10.5194/acp-12-6185-2012>, 2012.

605 Wadleigh, M. A.: Sulphur isotopic composition of aerosols over the western North Atlantic Ocean, in:  
606 *Canadian Journal of Fisheries and Aquatic Sciences*, <https://doi.org/10.1139/F04-073>, 2004.

607 Winiger, P., Andersson, A., Yttri, K. E., Tunved, P., and Gustafsson, Ö.: Isotope-Based Source  
608 Apportionment of EC Aerosol Particles during Winter High-Pollution Events at the Zeppelin  
609 Observatory, Svalbard, *Environ. Sci. Technol.*, 49, <https://doi.org/10.1021/acs.est.5b02644>, 2015.

610 World Health Organization: WHO global air quality guidelines: particulate matter (PM<sub>2.5</sub> and  
611 PM<sub>10</sub>), ozone, nitrogen dioxide, sulfur dioxide and carbon monoxide, 2021.

612

613

614